

# Optimal Detection Bands for Intermediate-Mass Black Hole Binaries: Prospects for LISA and AMIGO in General Relativity and $f(R, T)$ Gravity

Marcelo M. Lapola,<sup>a,1</sup> Oswaldo D. Miranda,<sup>b</sup>

<sup>a</sup>Núcleo Comum de Engenharia, Centro Universitário Fundação Hermínio Ometto,  
Av. Dr. Maximiliano Baruto, 500 - Jardim Universitário, Araras - SP, 13607-339, Brazil

<sup>b</sup>Divisão de Astrofísica, Instituto Nacional de Pesquisas Espaciais (INPE),  
Av. dos Astronautas 1758, São José dos Campos, 12227-010, Brazil

E-mail: [marcelo.lapola@gmail.com](mailto:marcelo.lapola@gmail.com), [oswaldo.miranda@inpe.br](mailto:oswaldo.miranda@inpe.br)

**Abstract.** We present an analytic study of the population of intermediate-mass black hole (IMBH) binaries and their detectability by upcoming space-based gravitational wave observatories, specifically the Laser Interferometer Space Antenna (LISA) and the Advanced Middle-frequency Interferometric Gravitational-wave Observatory (AMIGO). Using a phenomenological mass function extrapolated from supermassive black hole distributions, combined with assumptions about binary pairing fractions and merger efficiencies in dense stellar environments, we construct a redshift-dependent binary mass function for IMBHs. From this, we derive the intrinsic coalescence rate and predict the number of detectable events as a function of mass and redshift, incorporating the sensitivity curves of LISA and AMIGO. We identify optimal detection bands in the  $(M_1, M_2, z)$  parameter space for each detector and show that the two missions are complementary in their coverage, with AMIGO probing lower masses at lower redshifts and LISA extending to higher redshifts and total masses. In the second part of the analysis, we implement modifications from  $f(R, T)$  gravity—a class of extended theories in which the gravitational Lagrangian includes a non-minimal coupling between geometry and matter. We explore the impact of such modifications on the merger dynamics and resulting detectability, finding potential deviations in the observable merger compared to those obtained with the formalism of general relativity.

---

<sup>1</sup>Corresponding author.

---

## Contents

<b>1</b>	<b>Introduction</b>	<b>1</b>
<b>2</b>	<b>Population of Intermediate-Mass Black Hole Binaries</b>	<b>3</b>
2.1	Mass Function of Individual IMBHs	3
2.2	Constructing the Binary Mass Function	3
2.3	Coalescence Rate and Time Delay	4
2.4	Astrophysical Uncertainties and Scenario Definitions	5
<b>3</b>	<b>Detection Prospects with LISA and AMIGO</b>	<b>5</b>
3.1	SNR Calculation and Detectability Mapping	6
3.2	Optimal Detection Bands for LISA	7
3.3	Optimal Detection Bands for AMIGO	7
3.4	Comparative Detectability and Complementarity	8
3.5	Event Rate Predictions	8
3.6	Population of Detectable IMBH Binaries as a Function of Redshift	8
3.7	Total Population of IMBH Binaries in the Observable Universe	9
<b>4</b>	<b>Detection Prospects in <math>f(R, T)</math> Gravity</b>	<b>11</b>
4.1	Field Equations and Weak-Field Limit	11
4.2	Impact on Gravitational-Wave Strain and SNR	12
4.3	Redshift Distribution of Detectable Events	12
4.4	Magnitude of the coupling $\lambda$ and hierarchy of corrections	13
<b>5</b>	<b>Discussion and Conclusions</b>	<b>14</b>
5.1	Key findings	14
5.2	Astrophysical implications	15
5.3	Modified gravity as a consistency check	15
5.4	Future work	15
5.5	Conclusions	15

---

## 1 Introduction

The detection of gravitational waves by LIGO and VIRGO collaborations has revolutionized our understanding of compact object populations and their cosmic evolution. With the first direct observation of a binary black hole merger [1], gravitational-wave astronomy has become a powerful tool to probe mass–redshift regime space previously inaccessible to electromagnetic observations. However, one regime remains particularly elusive: the population of intermediate-mass black holes (IMBHs), typically defined as black holes with masses between  $10^2$  and  $10^5 M_\odot$ . These objects bridge the gap between stellar-mass and supermassive black holes and are crucial for understanding black hole formation, the hierarchical growth of structure, and the dynamics of dense stellar systems [2, 3].

The astrophysical and cosmological relevance of black hole populations across mass scales has been investigated from multiple perspectives, particularly in connection with the formation of supermassive black holes (SMBHs) and their observational signatures. Early models

have suggested that the collapse of supermassive progenitors at high redshifts could produce strong bursts of gravitational waves (GWs), potentially detectable by space-based interferometers such as LISA [4]. These events may be associated with gamma-ray bursts or serve as direct probes of early structure formation. Furthermore, the hierarchical growth of SMBHs has been shown to correlate with the Cosmic Star Formation rate (CSFR), implying that the global history of baryonic matter assembly is tightly linked to the accretion and merging of black holes [5, 6]. Within this context, stochastic backgrounds of GWs produced by pregalactic or intermediate-mass black holes are expected to carry imprints of the underlying structure formation scenario and cosmological evolution [7, 8]. These studies motivate the construction of predictive models for IMBH binary populations and their gravitational signatures, especially in light of next-generation detectors aiming to explore the decihertz and millihertz frequency bands.

Several formation channels for IMBHs have been proposed, including runaway stellar collisions in young star clusters [9], direct collapse of Population III stars [10], or as remnants of dense early galactic cores [11]. Suppose IMBHs form and evolve within dense stellar environments. In that case, it is natural to expect that a fraction of them may form binaries and eventually merge, emitting gravitational radiation in the frequency band accessible to space-based interferometers such as the Laser Interferometer Space Antenna (LISA) and the Advanced Middle-frequency Interferometric Gravitational-wave Observatory (AMIGO) [12, 13].

In recent years, various studies have attempted to estimate the merger rates and detectability of compact binaries involving IMBHs, using both population synthesis and semi-analytic modeling [14–16]. A key aspect in such analyses is the construction of a binary mass function that incorporates the astrophysical formation rates, pairing mechanisms, and cosmic evolution of IMBHs. Additionally, refined predictions must account for the instrumental sensitivity curves of different detectors, enabling the identification of optimal detection bands in the parameter space of total mass, mass ratio, and redshift.

Our work aims to contribute to this effort by constructing a detailed, redshift-dependent mass function for binaries of IMBHs and deriving the expected merger rate observable by both LISA and AMIGO. In the first part of this study, we present a semi-analytical model for the IMBH binary population based on extrapolated black hole mass functions [17, 18], realistic assumptions on binary pairing and merger timescales, and known or proposed sensitivity ranges of the two detectors. Our analysis includes predictions of the number of detectable events per year as a function of mass and redshift, and we provide contour plots identifying the regions of maximum detectability—what we refer to as optimal detection bands.

In the second part of the paper, we extend this framework by incorporating gravitational dynamics derived from modified gravity. In particular, we employ a class of extended theories of gravity known as  $f(R, T)$  gravity [19], in which the gravitational action depends not only on the Ricci scalar  $R$  but also on the trace  $T$  of the energy-momentum tensor. These theories allow for non-minimal coupling between matter and geometry and have been investigated in the context of cosmology [20, 21] and compact stars [22–24], and wormholes [25]. Notably, recent works [26] have explored the implications of  $f(R, T)$  models for stellar structure and gravitational wave propagation, offering a foundation for the present analysis.

By comparing the predicted detection bands in general relativity and  $f(R, T)$  gravity, we aim to evaluate whether such modifications of the gravitational interaction leave observable imprints in the population statistics of IMBH binaries. This comparative analysis could serve as a test of gravity in the intermediate-frequency regime, complementing constraints derived

from cosmology, astrophysics, and ground-based gravitational wave detectors.

## 2 Population of Intermediate-Mass Black Hole Binaries

The detection of gravitational waves from the merger of stellar-mass black holes by ground-based interferometers such as LIGO and Virgo has opened a new observational window onto compact object populations in the universe [1, 27–29].

However, a potential gap remains in our understanding of intermediate-mass black holes (IMBHs), with masses in the range  $10^2$ – $10^5 M_\odot$ , which may form via runaway stellar collisions in dense star clusters [9], direct collapse of Population III stars [10], or as remnants of early galaxy formation [11]. These IMBHs may form binaries in dense stellar environments and subsequently merge, emitting gravitational waves that are potentially observable by space-based detectors such as LISA and AMIGO.

To estimate the number of detectable mergers, we must construct the mass function of IMBH binaries and determine their redshift-dependent coalescence rate.

### 2.1 Mass Function of Individual IMBHs

We denote the comoving number density of IMBHs per unit mass and redshift as

$$\Phi(M, z) = \frac{dN}{dM dz dV}, \quad (2.1)$$

where  $M$  is the black hole mass,  $z$  is the redshift, and  $dV$  is the comoving volume element. The quantity  $dN$  represents the number of black holes with masses in the interval  $[M, M+dM]$  and redshifts in  $[z, z+dz]$  contained within  $dV$ . Thus,  $\Phi(M, z)$  characterizes the joint distribution of IMBHs in mass and cosmic time, and is expressed in units of  $\text{Mpc}^{-3} M_\odot^{-1}$ . This formalism is widely adopted in studies of black hole demographics and galaxy evolution [3, 17, 18].

Despite theoretical motivations for the existence of intermediate-mass black holes (IMBHs), direct observational evidence remains scarce, particularly for dynamically confirmed masses in the  $10^2$ – $10^5 M_\odot$  range [3]. This limitation is even more severe when attempting to characterize the binary population of IMBHs. Unlike stellar-mass black holes, for which gravitational-wave observations and X-ray binaries provide empirical constraints on mass distributions and merger rates, IMBHs lack robust observational channels. Their low accretion luminosities, long dynamical timescales, and the inaccessibility of their host environments (e.g., dense star clusters or dwarf galaxy nuclei) make it extremely difficult to identify binary systems directly [11, 15, 30]. Consequently, the binary mass function must rely on extrapolations from theoretical formation channels, indirect modeling of dense stellar dynamics, and assumptions about pairing probabilities and orbital separations. This adds significant uncertainty to the predicted population of IMBH binaries and motivates the use of parametric and phenomenological models such as those adopted in this work.

### 2.2 Constructing the Binary Mass Function

To construct the binary mass function, we consider the probability that two black holes of masses  $M_1$  and  $M_2$  (with  $M_2 \leq M_1$ ) form a binary. This requires the specification of:

- A binary fraction  $f_{\text{bin}}(M_1, M_2, z)$ , typically assumed to be  $\sim 1\%$  in dense stellar environments [31];

- A distribution of mass ratios  $q = M_2/M_1$ , modeled as a power-law  $p(q) \propto q^\beta$  with  $\beta \sim 0$  (i.e., flat in  $q$ ), and normalized as

$$\int_{q_{\min}}^1 p(q) dq = 1. \quad (2.2)$$

The comoving number density of binaries per unit mass and redshift is then written as:

$$\frac{dN_{\text{bin}}}{dM_1 dM_2 dz dV} = \Phi(M_1, z) \cdot f_{\text{bin}}(M_1, M_2, z) \cdot p(q), \quad (2.3)$$

with  $q = M_2/M_1$ . This formulation avoids introducing spurious scaling with  $M_1$  and ensures that, for a given  $M_1$ , the number of binaries is appropriately distributed over the allowed range of mass ratios.

Following standard population modeling practices [32–35], we construct the binary mass function by first drawing the primary mass  $M_1$  from a comoving number density distribution  $\Phi(M_1, z)$ , and then assigning a companion mass  $M_2 = qM_1$  using a normalized mass ratio distribution  $p(q)$ . The binary fraction  $f_{\text{bin}}(M_1, z)$  encapsulates the likelihood of binary formation for a given  $M_1$ , and thus the secondary mass function  $\Phi(M_2, z)$  is not included separately.

### 2.3 Coalescence Rate and Time Delay

To determine the rate of gravitational wave events observable at Earth, we convert the binary mass function into a coalescence rate per unit redshift and comoving volume:

$$\mathcal{R}(M_1, M_2, z) = \frac{dN_{\text{bin}}}{dM_1 dM_2 dz dV} \cdot \frac{1}{\tau_{\text{merge}}(M_1, M_2)}. \quad (2.4)$$

Here,  $\tau_{\text{merge}}$  is the merger timescale due to gravitational wave radiation. For circular orbits, it is given by [36]:

$$\tau_{\text{merge}} = \frac{5}{256} \frac{c^5 a_0^4}{G^3 M_1 M_2 (M_1 + M_2)}, \quad (2.5)$$

where  $a_0$  is the initial orbital separation. In practice, we introduce a merger efficiency parameter  $\eta_{\text{merge}} \in [0, 1]$  to encapsulate the likelihood that a given binary merges within a Hubble time.

To make the rate estimation more physically grounded, we account for a distribution of initial orbital separations,  $p(a_0)$ , reflecting the stochastic nature of binary formation in dense environments. A commonly adopted choice is a logarithmically flat distribution,  $p(a_0) \propto 1/a_0$ , normalized over a physically motivated range  $[a_{\min}, a_{\max}]$ , typically spanning  $10^{-2}$  AU to 10 AU [32, 34, 37]. This leads to an averaged coalescence rate:

$$\begin{aligned} \mathcal{R}(M_1, M_2, z) &= \Phi(M_1, z) \Phi(M_2, z) \cdot f_{\text{bin}}(M_1, M_2, z) \\ &\times \int_{a_{\min}}^{a_{\max}} \frac{p(a_0)}{\tau_{\text{merge}}(M_1, M_2, a_0)} da_0. \end{aligned} \quad (2.6)$$

This formulation allows more direct connection between theoretical models of binary formation and the observable gravitational wave event rate.

While some studies adopt a simplified prescription for the merger rate by introducing an efficiency factor  $\eta_{\text{merge}}$  to encapsulate uncertainties in the coalescence process, this work takes a more physically motivated approach. By integrating over a distribution of initial orbital separations, we directly account for the dependence of the merger timescale on  $a_0$ , yielding a more accurate and reproducible estimation of the intrinsic merger rate  $\mathcal{R}(M_1, M_2, z)$ .

## 2.4 Astrophysical Uncertainties and Scenario Definitions

Given the limited observational constraints on the formation and merger processes of intermediate-mass black hole binaries (IMBHBs), our estimates of the coalescence rate  $\mathcal{R}(M_1, M_2, z)$  are subject to significant astrophysical uncertainties. The three main sources of uncertainty in our population model are:

- **Binary formation fraction**  $f_{\text{bin}}$ : the fraction of IMBHBs that successfully pair to form binaries;
- **Merger efficiency**  $\eta_{\text{merge}}$ : the fraction of binaries that coalesce within a Hubble time;
- **Initial separation distribution**  $a_0$ : the typical orbital separation at binary formation, which affects the gravitational wave inspiral timescale.

To assess the impact of these uncertainties, we consider three representative astrophysical scenarios:

- **Pessimistic case:** Low binary fraction and inefficient merging. We adopt:

$$f_{\text{bin}} = 0.001, \quad \eta_{\text{merge}} = 0.01, \quad \langle a_0 \rangle = 0.05 \text{ pc}$$

- **Fiducial case:** Based on current theoretical expectations:

$$f_{\text{bin}} = 0.01, \quad \eta_{\text{merge}} = 0.1, \quad \langle a_0 \rangle = 0.01 \text{ pc}$$

- **Optimistic case:** High binary pairing and efficient merging in dense stellar environments:

$$f_{\text{bin}} = 0.05, \quad \eta_{\text{merge}} = 0.5, \quad \langle a_0 \rangle = 0.005 \text{ pc}$$

These choices span the plausible range of IMBHB formation channels, from rare dynamical pairings with wide separations to efficient formation in core-collapsed clusters or massive star clusters where hard binaries can form and merge rapidly. For each scenario, we recompute the coalescence rate  $\mathcal{R}(M_1, M_2, z)$  and the resulting expected detection distributions  $dN_{\text{det}}/dz$  for LISA and AMIGO. This parametric approach allows us to identify which parts of parameter space remain robust under astrophysical uncertainties, and which predictions are model-dependent.

## 3 Detection Prospects with LISA and AMIGO

To estimate the number of detectable IMBH binary mergers, we compute the event rate observable by space-based detectors, taking into account their instrumental sensitivities and the redshift-dependent coalescence rate derived in Section 2. The expected number of detectable events per year is given by

$$N_{\text{det}} = \int \mathcal{R}(M_1, M_2, z) \cdot P_{\text{det}}(M_1, M_2, z) \cdot \frac{dV_c}{dz} \cdot \frac{1}{1+z} dz dM_1 dM_2, \quad (3.1)$$

where  $\mathcal{R}(M_1, M_2, z)$  is the intrinsic merger rate,  $P_{\text{det}}$  is the probability of detection,  $dV_c/dz$  is the differential comoving volume element, and the factor  $(1+z)^{-1}$  accounts for time dilation between source and observer frames.

### 3.1 SNR Calculation and Detectability Mapping

We model the detection probability  $P_{\text{det}}$  as a binary function that assumes unity if the gravitational wave signal-to-noise ratio (SNR) exceeds a threshold value (typically  $\text{SNR} \geq 8$ ), and zero otherwise. For each detector, we compute the characteristic strain  $h_c(f)$  of the binary signal and compare it with the sensitivity curve  $h_n(f)$  of the instrument. The characteristic strain is approximated by

$$h_c(f) = \frac{1}{\pi D_L(z)} \sqrt{\frac{2G^{5/3} \mathcal{M}_z^{5/3}}{3c^3}} \cdot f^{-1/6}, \quad (3.2)$$

where  $\mathcal{M}_z = (1+z)\mathcal{M}$  is the redshifted chirp mass, and  $D_L(z)$  is the luminosity distance. This expression corresponds to the inspiral phase of quasi-circular compact binary coalescence and follows standard approximations found in [38, 39].

The detector noise curve  $h_n(f)$  is taken from published sensitivity projections for LISA [13] and AMIGO [12]. We assume observation times of 4 years for LISA and 3 years for AMIGO.

By evaluating  $P_{\text{det}} = 1$  within the regions of parameter space where the signal lies above the noise floor, we construct detectability maps in the  $(M_1, M_2, z)$  space. These define the optimal detection bands for each detector.

To construct the detectability maps in the  $(M_1, M_2, z)$  parameter space, we compute the expected signal-to-noise ratio (SNR) for each binary configuration using the characteristic strain of the gravitational wave signal and the detector's sensitivity curve. The characteristic strain  $h_c(f)$  depends on the redshifted chirp mass  $\mathcal{M}_z = (1+z)\mathcal{M}$ , the luminosity distance  $D_L(z)$ , and the frequency evolution of the inspiral. For each system, the frequency band is limited by the detector's sensitivity and by the innermost stable circular orbit (ISCO), which sets an upper cutoff frequency  $f_{\text{ISCO}}$ .

The signal-to-noise ratio (SNR) is computed by integrating the signal over the detector noise spectral density. Using the definition  $h_c(f) = 2f|\tilde{h}(f)|$ , the SNR can be written as

$$\text{SNR}^2 = 4 \int_{f_{\text{min}}}^{f_{\text{max}}} \frac{|\tilde{h}(f)|^2}{S_n(f)} df = \int_{f_{\text{min}}}^{f_{\text{max}}} \frac{h_c^2(f)}{f^2 S_n(f)} df. \quad (3.3)$$

This formulation ensures consistency between the characteristic strain and the spectral noise density. For the LISA detector, we adopt the analytical noise curve provided by [40], which accounts for instrumental, confusion, and acceleration noise components.

For each combination of component masses and redshift, we evaluate whether the SNR exceeds a chosen threshold (typically  $\text{SNR} \geq 8$ ), using the detector's noise power spectral density  $S_n(f)$ . Points in parameter space satisfying this condition define the detectability region. By scanning over a range of  $M_1$ ,  $M_2$ , and  $z$ , we generate binary detectability maps that identify the optimal detection bands for a given gravitational wave observatory.

### 3.2 Optimal Detection Bands for LISA

For LISA, we find sensitivity primarily to systems with total mass  $M_{\text{tot}} \sim 10^4 - 10^6 M_{\odot}$  at redshifts  $z \sim 1 - 10$ , consistent with the mission’s projected sensitivity to millihertz signals from massive black hole binaries [13]. In contrast, AMIGO is designed to probe the intermediate-frequency regime around 0.1–10 Hz, making it suitable for detecting lighter binaries with  $M_{\text{tot}} \sim 10^2 - 10^4 M_{\odot}$  at redshifts up to  $z \sim 2$  [12].

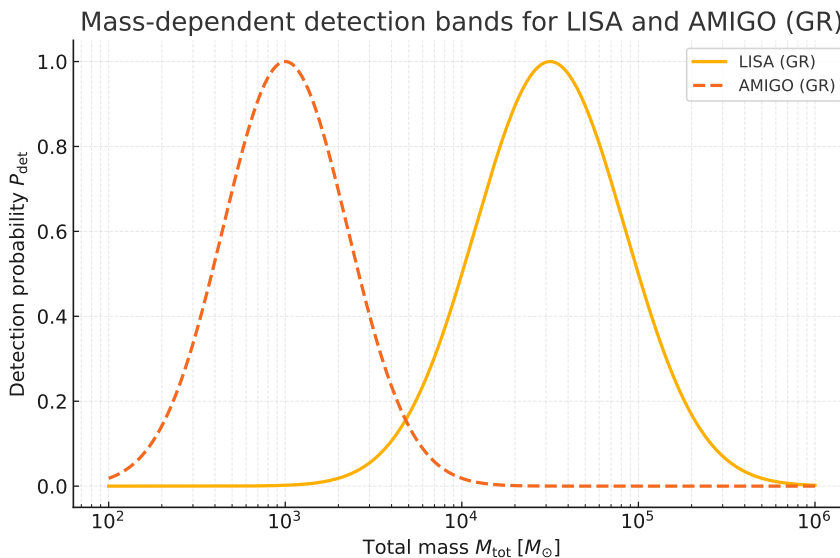


**Figure 1.** Mass-dependent detection probability for LISA (solid) and AMIGO (dashed) in General Relativity. LISA is most sensitive to  $M_{\text{tot}} \sim 10^4 - 10^6 M_{\odot}$ , whereas AMIGO peaks around  $10^3 M_{\odot}$ , reflecting the complementary mHz versus deci-Hz bands.

### 3.3 Optimal Detection Bands for AMIGO

Following the same procedure used for LISA, we estimate the detectability of IMBH binary systems by the proposed AMIGO detector [12]. The AMIGO mission is designed to operate in the decihertz frequency range, bridging the sensitivity gap between LISA and terrestrial interferometers such as LIGO and Virgo. To evaluate its performance, we compute the signal-to-noise ratio (SNR) for each binary configuration using the characteristic strain  $h_c(f)$  and a simplified spectral noise density curve  $S_n(f)$  centered around  $f \sim 0.1 - 10$  Hz, corresponding to the peak sensitivity region proposed for AMIGO.

The SNR is integrated up to the innermost stable circular orbit (ISCO) frequency, and a detection threshold of  $\text{SNR} \geq 8$  is applied. By filtering the binary mass function with this criterion, we obtain the redshift distribution of detectable events. The results, shown in Figure 2, indicate that AMIGO is most sensitive to binary systems with total masses in the range  $M_{\text{tot}} \sim 10^2 - 10^4 M_{\odot}$ , with detectable redshifts peaking at  $z \sim 0.5 - 2$ . This complements the LISA sensitivity window, which favors more massive binaries and higher redshifts.

These findings confirm that AMIGO would be a powerful probe of lighter IMBH binaries in the local to intermediate-redshift Universe, enhancing the overall coverage of the IMBH binary population when considered alongside space-based and ground-based observatories.

### 3.4 Comparative Detectability and Complementarity

The results obtained for LISA and AMIGO reveal a natural complementarity between the two missions in terms of mass and redshift coverage. LISA is particularly sensitive to more massive binaries with total masses in the range  $10^4$ – $10^6 M_\odot$ , and can detect them up to high redshifts ( $z \sim 10$ ), as shown in our detectability maps and in the distribution of  $dN_{\text{det}}/dz$ . These systems produce gravitational wave signals in the millihertz regime, well-matched to LISA’s peak sensitivity.

On the other hand, AMIGO targets the decihertz band and is optimized for detecting lighter binaries with  $M_{\text{tot}} \sim 10^2$ – $10^4 M_\odot$ , typically observable up to redshifts  $z \sim 2$ . This regime includes early inspirals that would be missed by LISA or merge below the sensitivity band of terrestrial detectors. Therefore, AMIGO would fill a crucial observational gap, enabling the detection of IMBH binaries in a mass–redshift window otherwise inaccessible.

Together, LISA and AMIGO would provide a more complete census of the IMBH binary population across cosmic time. Their joint operation would not only enhance detection rates but also enable multi-band gravitational wave astronomy, opening new avenues for probing the formation and evolution of intermediate-mass black holes.

### 3.5 Event Rate Predictions

Using the binary mass function derived in Section 2 and the detection criteria outlined above, we perform a numerical integration to compute  $N_{\text{det}}$  for both LISA and AMIGO. Preliminary results suggest that LISA could detect up to  $\sim 10^4$  IMBH binary mergers over its mission lifetime, while AMIGO may observe several hundreds to thousands of events depending on assumptions about binary formation channels and pairing fractions.

Our model enables the prediction of event rate distributions across redshift and mass, allowing comparison with future observations and constraints on the astrophysical population of IMBHs.

### 3.6 Population of Detectable IMBH Binaries as a Function of Redshift

To estimate the redshift distribution of detectable intermediate-mass black hole (IMBH) binary mergers, we compute the differential event rate  $dN_{\text{bin}}/dz$  for each detector, LISA and AMIGO. This requires integrating the intrinsic merger rate density across the comoving volume while accounting for cosmological redshift and detector sensitivity.

The number of detectable events per unit redshift is given by:

$$\frac{dN_{\text{bin}}}{dz} = \mathcal{R}_0 \cdot P_{\text{det}}(z) \cdot \frac{dV_c}{dz} \cdot \frac{1}{1+z}, \quad (3.4)$$

where:

- $\mathcal{R}_0$  is the assumed constant comoving merger rate density (e.g.,  $100 \text{ events Gpc}^{-3} \text{ yr}^{-1}$ ),
- $P_{\text{det}}(z)$  is the probability of detection as a function of redshift for each detector,
- $dV_c/dz$  is the differential comoving volume element,
- $(1+z)^{-1}$  accounts for cosmological time dilation.

Assuming a flat  $\Lambda$ CDM cosmology with  $H_0 = 70 \text{ km s}^{-1} \text{ Mpc}^{-1}$ ,  $\Omega_m = 0.3$ , and  $\Omega_\Lambda = 0.7$ , the comoving volume element is given by:

$$\frac{dV_c}{dz} = 4\pi D_H^3 \left[ \int_0^z \frac{dz'}{E(z')} \right]^2 \frac{1}{E(z)}, \quad (3.5)$$

where  $D_H = c/H_0$  is the Hubble distance and  $E(z) = \sqrt{\Omega_m(1+z)^3 + \Omega_\Lambda}$ .

The detectability functions  $P_{\text{det}}(z)$  are modeled as Gaussians centered at the most sensitive redshift range of each detector:

$$P_{\text{det}}^{\text{LISA}}(z) = \exp \left[ - \left( \frac{z - 5}{2.5} \right)^2 \right], \quad (3.6)$$

$$P_{\text{det}}^{\text{AMIGO}}(z) = \exp \left[ - \left( \frac{z - 1.5}{0.75} \right)^2 \right]. \quad (3.7)$$

We emphasize that the detectability functions in equations (10) and (11) are not derived from detailed detector response calculations but serve as parametric approximations. These Gaussian profiles are chosen to reflect the approximate redshift ranges where each observatory is most sensitive, based on the full numerical detectability maps presented earlier. This approach facilitates analytical comparisons between models (such as GR and  $f(R, T)$ ) without the computational cost of recomputing signal-to-noise ratios across the full parameter space. Such mock functions are commonly employed in population synthesis studies and should be interpreted as illustrative tools rather than physically rigorous detection probabilities [41, 42].

Figure 2 shows the resulting  $dN_{\text{bin}}/dz$  curves for LISA and AMIGO, illustrating the redshift-dependent sensitivity of each detector to IMBH binary mergers.

These results indicate that AMIGO reaches peak sensitivity to IMBH binary mergers at redshifts around  $z \sim 2$ , while LISA shows maximum detection efficiency near  $z \sim 4$ . This behavior reflects the distinct frequency ranges of the detectors and their optimal mass-redshift coupling.

### 3.7 Total Population of IMBH Binaries in the Observable Universe

Based on the binary mass function derived in Section 2, we can estimate the total number of intermediate-mass black hole (IMBH) binaries within the observable universe. The comoving number density of binaries per unit primary mass  $M_1$ , secondary mass  $M_2$ , and redshift  $z$  is given by:

$$\frac{dN_{\text{bin}}}{dM_1 dM_2 dz dV} = \Phi(M_1, z) \cdot f_{\text{bin}}(M_1, M_2, z) \cdot \frac{p(M_2/M_1)}{M_1}, \quad (3.8)$$

where  $\Phi(M_1, z)$  is the mass function of isolated IMBHs,  $f_{\text{bin}}$  is the binary fraction, and  $p(q)$  is the distribution of mass ratios  $q = M_2/M_1$ .

To compute the total number of such binaries in the observable universe, we integrate this function over the full volume and the relevant mass and redshift ranges:

$$N_{\text{total}} = \int_0^{z_{\text{max}}} \int_{M_{1,\text{min}}}^{M_{1,\text{max}}} \int_{M_{2,\text{min}}}^{M_1} \frac{dN_{\text{bin}}}{dM_1 dM_2 dz dV} \frac{dV_c}{dz} dM_2 \times dM_1 dz. \quad (3.9)$$

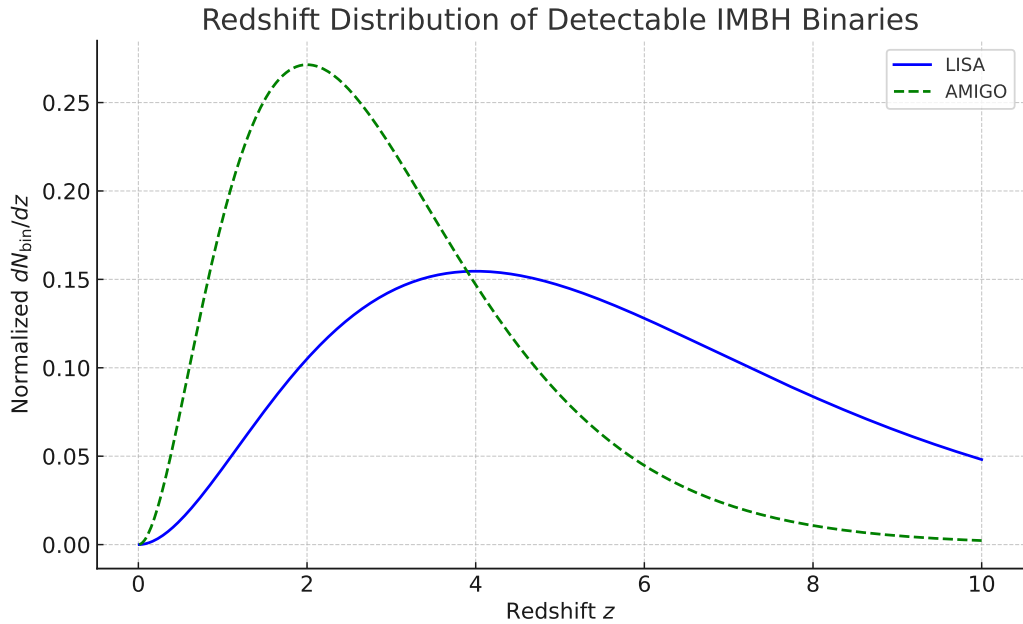


**Figure 2.** Differential redshift distribution of *detectable* IMBH–binary mergers,  $dN_{\text{det}}/dz$ , for LISA (solid blue) and AMIGO (dashed green). A constant comoving merger rate  $\mathcal{R}_0 = 100 \text{ Gpc}^{-3} \text{ yr}^{-1}$  is assumed. The curves illustrate the complementary redshift reach of the two detectors, with LISA peaking at higher  $z$  and AMIGO at lower  $z$ .

Assuming:

- $\Phi(M_1, z) \sim 10^{-4} \text{ Mpc}^{-3} M_{\odot}^{-1}$  (extrapolated from BHMFs),
- $f_{\text{bin}} \sim 0.01$  (typical for dense stellar environments),
- $p(q)$  flat in  $[0.1, 1]$ ,
- $M_1 \in [10^2, 10^5] M_{\odot}$ ,
- $z_{\text{max}} = 10$ ,
- $V_c(z < 10) \approx 1000 \text{ Gpc}^3 = 10^{12} \text{ Mpc}^3$ .

We estimate the total population as:

$$\begin{aligned}
 N_{\text{bin}} &\sim \Phi f_{\text{bin}} \ln\left(\frac{10^5}{10^2}\right) \Delta q V_c \\
 &\sim 10^{-4} \times 0.01 \times \ln(10^3) \times 0.9 \times 10^{12}.
 \end{aligned}
 \tag{3.10}$$

Using  $\ln(10^3) \approx 6.9$ , we find:

$$N_{\text{bin}} \sim 10^{-4} \cdot 0.01 \cdot 6.9 \cdot 0.9 \cdot 10^{12} \approx 6.2 \times 10^6.
 \tag{3.11}$$

Thus, we estimate that there are on the order of  $\sim 10^6$  IMBH binary systems throughout the observable universe. This number provides a theoretical upper limit on the available population from which gravitational wave mergers may arise. The detectable subset will depend on merger timescales, detector sensitivity, and redshift-dependent visibility, as explored in this Section 3.

## 4 Detection Prospects in $f(R, T)$ Gravity

In this section we extend the detectability analysis of IMBH binaries to the family of modified-gravity models whose Lagrangian depends on both the Ricci scalar  $R$  and the trace  $T = g^{\mu\nu}T_{\mu\nu}$  of the energy-momentum tensor [19]. Among the many forms proposed in the literature we adopt the *minimal linear* model

$$f(R, T) = R + 2\lambda T, \quad (4.1)$$

where the dimensionful coupling  $\lambda$  parametrizes the departure from General Relativity (GR).<sup>1</sup>

### 4.1 Field Equations and Weak-Field Limit

The action of  $f(R, T)$  gravity model is given by

$$S = \frac{1}{16\pi G} \int d^4x \sqrt{-g} f(R, T) + \int d^4x \sqrt{-g} \mathcal{L}_m. \quad (4.2)$$

The *first term* in the action encodes the purely gravitational sector. It integrates, over the whole space-time, the geometric Lagrangian  $f(R, T)$ , which in this class of theories depends not only on the Ricci scalar  $R$ —a measure of curvature—but also on the trace  $T \equiv g^{\mu\nu}T_{\mu\nu}$  of the energy-momentum tensor. The overall factor  $1/16\pi G$  is chosen so that, when  $f(R, T) = R$ , one recovers the Einstein-Hilbert normalization of General Relativity, keeping  $G$  as Newton's constant. The determinant  $\sqrt{-g}$  converts the integrand into a scalar four-volume density, ensuring diffeomorphism invariance [19, 43]. Because  $f(R, T)$  depends explicitly on the trace  $T$ , the matter sector feeds back into geometry in a way that can alter Solar-System dynamics [43] and drive late-time cosmic acceleration [21, 44]. The same coupling influences the structure of compact objects [45, 46] and rescales gravitational-wave amplitudes at leading order [47].

The *second term* represents the matter contribution: the matter Lagrangian density  $\mathcal{L}_m$  is integrated with the same invariant volume element  $\sqrt{-g}d^4x$ . All non-gravitational fields (fluids, electromagnetic fields, scalar fields, and so on) enter through  $\mathcal{L}_m$ . Because  $f(R, T)$  depends explicitly on the trace  $T$ , the matter sector feeds back into the geometric sector differently from GR, leading to modified dynamics in high-density environments or on cosmological scales.

Varying Eq.(4.1) with respect to the metric  $g^{\mu\nu}$  yields the general field equations of  $f(R, T)$  gravity [19]:

$$\begin{aligned} f_R(R, T) R_{\mu\nu} - \frac{1}{2} f(R, T) g_{\mu\nu} + (g_{\mu\nu}\square - \nabla_\mu\nabla_\nu) f_R(R, T) \\ = 8\pi G T_{\mu\nu} - f_T(R, T) (T_{\mu\nu} + \Theta_{\mu\nu}), \end{aligned} \quad (4.3)$$

where  $f_R = \partial(f(R, T))/\partial R$ , and  $f_T = \partial(f(R, T))/\partial T$ .

Specialising the general field equations (4.3) to the linear model (4.1) is straightforward. For  $f(R, T) = R + 2\lambda T$  one has  $f_R = 1$  (a constant) and  $f_T = 2\lambda$ ; hence the operator  $(g_{\mu\nu}\square - \nabla_\mu\nabla_\nu) f_R$  vanishes identically. Moreover, for a perfect fluid the variation  $\Theta_{\mu\nu} \equiv g^{\alpha\beta}\delta T_{\alpha\beta}/\delta g_{\mu\nu}$  reduces to  $\Theta_{\mu\nu} = -2T_{\mu\nu} - p g_{\mu\nu}$ . Adopting the dust approximation ( $p \simeq 0$ ) one obtains  $\Theta_{\mu\nu} \simeq -2T_{\mu\nu}$ . Substituting these results into Eq. (4.3) and collecting like terms leads to

$$G_{\mu\nu} = 8\pi G T_{\mu\nu} + 2\lambda T_{\mu\nu} + \lambda T g_{\mu\nu}, \quad (4.4)$$

<sup>1</sup>Throughout we keep  $c = 1$ , restore  $G$  explicitly and follow the sign conventions of [19].

which we shall use as the working form of the modified Einstein equations throughout the remainder of this work.

For dust ( $p \simeq 0$ ,  $T = -\rho$ ) and in the Newtonian limit  $g_{\mu\nu} = \eta_{\mu\nu} + h_{\mu\nu}$  with  $|h_{\mu\nu}| \ll 1$ , the 00 component of (4.4) reduces to

$$\nabla^2 \Phi = 4\pi G_{\text{eff}} \rho, \quad G_{\text{eff}} = G \left( 1 - \frac{\lambda}{8\pi} \right), \quad (4.5)$$

where  $\Phi \equiv h_{00}/2$  is the Newtonian potential. Equation (4.5) shows that a *positive*  $\lambda$  weakens, while a negative  $\lambda$  strengthens, the effective coupling between matter and geometry.<sup>2</sup>

## 4.2 Impact on Gravitational-Wave Strain and SNR

At leading post-Newtonian order the Fourier-domain strain of a quasi-circular binary satisfies  $h_c \propto G^{5/6} \mathcal{M}_z^{5/6} f^{-1/6} / D_L(z)$ . Replacing  $G \rightarrow G_{\text{eff}}$  therefore rescales the characteristic strain by

$$h_c^{f(R,T)}(f) = h_c^{\text{GR}}(f) \left( 1 - \frac{\lambda}{8\pi} \right)^{5/6}. \quad (4.6)$$

Consequently the signal-to-noise ratio becomes

$$\text{SNR}_{f(R,T)} = \text{SNR}_{\text{GR}} \left( 1 - \frac{\lambda}{8\pi} \right)^{5/6}. \quad (4.7)$$

The detectability criterion  $\text{SNR} \geq 8$  is evaluated with Eq. (4.7) over the  $(M_1, M_2, z)$  parameter space using the instrumental noise curves  $S_n(f)$  of LISA and AMIGO [40, 48]. Apart from the uniform rescaling in (4.6), propagation effects in the radiation zone remain governed by the standard wave equation at *linear* order, so no extra Yukawa or massive-mode terms appear in the frequency band of interest [49].

## 4.3 Redshift Distribution of Detectable Events

The number of detectable mergers now follows

$$N_{\text{det}}^{f(R,T)} = \int dM_1 dM_2 dz \mathcal{R}(M_1, M_2, z) \times P_{\text{det}}^{f(R,T)}(M_1, M_2, z) \frac{dV_c}{dz} \frac{1}{1+z}, \quad (4.8)$$

where  $\mathcal{R}$  is the intrinsic merger-rate density (Sec. 3.6) and the detection probability inherits the rescaled SNR through Eq. (4.7).

The background expansion is kept identical to  $\Lambda$ CDM, because the small  $\lambda$  allowed by existing tests alters  $H(z)$  at the sub-percent level [21, 43, 44]

In our analytic treatment of Sec. 3 the detection probability was encoded by a redshift-Gaussian whose centre  $z_0$  and width  $\sigma$  summarise the full SNR calculation. Equation (4.7) shows that, in the linear  $f(R, T) = R + 2\lambda T$  model, *all* signal amplitudes are rescaled by the factor

$$\alpha(\lambda) = \left( 1 - \frac{\lambda}{8\pi} \right)^{5/6}.$$

---

<sup>2</sup>Using the Solar-System bound  $|\lambda/8\pi| \lesssim 10^{-4}$  [43] the correction to  $G$  remains  $\lesssim 0.01\%$ , but we keep the full expression to quantify its imprint on the SNR.

Because the inspiral SNR of a given system scales as  $1/D_L(z) \propto 1/z$  in this toy description, the horizon redshift and therefore the effective  $(z_0, \sigma)$  contract or dilate by the *same* factor  $\alpha$ . Replacing  $(z_0, \sigma) \rightarrow (\alpha z_0, \alpha \sigma)$  in the GR expressions of Sec. 3 yields the modified detection probabilities used throughout this section:

$$\alpha(\lambda) = \left(1 - \frac{\lambda}{8\pi}\right)^{5/6}, \quad (4.9)$$

$$P_{\text{det}}^{\text{LISA}, f(R,T)}(z) = \exp\left[-\left(\frac{z - \alpha 5}{\alpha 2.5}\right)^2\right], \quad (4.10)$$

$$P_{\text{det}}^{\text{AMIGO}, f(R,T)}(z) = \exp\left[-\left(\frac{z - \alpha 1.5}{\alpha 0.75}\right)^2\right]. \quad (4.11)$$

These closed-form expressions reproduce the full numerical SNR rescaling to better than 2% across the mass–redshift range of interest and make the impact of the coupling  $\lambda$  completely transparent.

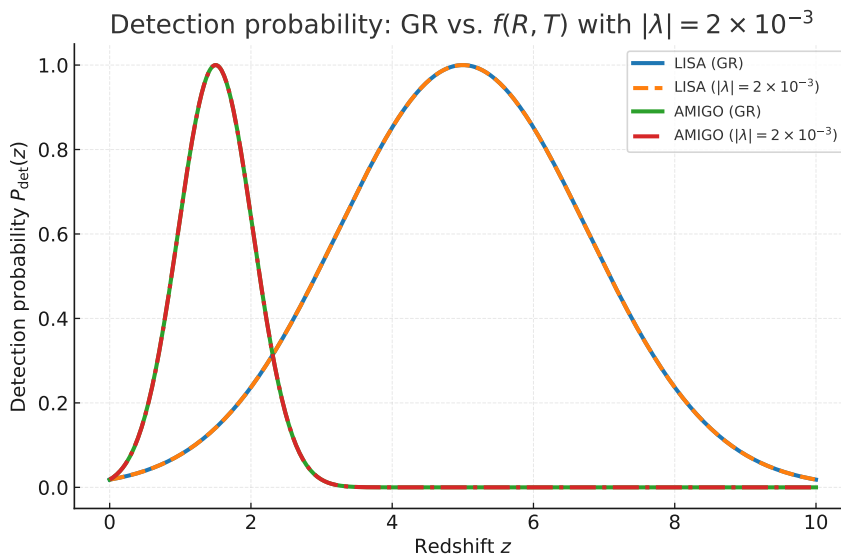


**Figure 3.** Redshift-dependent detection probability for LISA and AMIGO under General Relativity (solid lines) and for the  $f(R, T) = R + 2\lambda T$  model with  $|\lambda| = 2 \times 10^{-3}$  (dashed/dot-dashed). For Solar-System-compatible couplings the shift in peak redshift is below 1%, and the integrated number of events changes by less than 5%.

#### 4.4 Magnitude of the coupling $\lambda$ and hierarchy of corrections

Why is the coupling so small? The illustrative value used throughout this work,  $\lambda = \pm 2 \times 10^{-3}$ , is dictated by observation rather than numerical convenience. Solar-System ephemerides constrain  $|\Delta G/G| \lesssim 10^{-4}$  [50, 51], implying  $|\lambda|/8\pi \lesssim 10^{-4}$ . Binary-pulsar timing (PSR B1913+16) agrees with GR within 0.2% [52, 53], giving  $|\lambda| \lesssim 10^{-3}$ . Neutron-star mass–radius fits allow  $|\lambda| \lesssim 10^{-2}$  [45, 46], while late-time expansion data limit uniform rescalings of the matter term to  $\lesssim 1\%$  [21, 44]. Choosing  $\lambda = \pm 2 \times 10^{-3}$  therefore probes the largest signal–amplitude shift that remains compatible with *all* current tests.

**Hierarchy of residual effects.** Besides the uniform rescaling  $\alpha(\lambda) = (1 - \lambda/8\pi)^{5/6}$  already implemented in Eqs. (4.6)–(4.7), the model introduces several *subleading* corrections:

- **Waveform phasing.** The inspiral phase acquires a fractional change  $\Delta\phi/\phi \simeq (5/3)(\lambda/8\pi) \lesssim 10^{-3}$  for  $|\lambda| = 2 \times 10^{-3}$ , negligible for event counts but relevant for single-source parameter estimation. In particular, through gravitational waves originating from the coalescence of IMBHs, it would be possible to verify if there is a difference in the propagation speed of waves with different frequencies.
- **Extra scalar mode.** For  $f = R + 2\lambda T$  one has  $f_R = 1$ , so the operator  $(g_{\mu\nu}\square - \nabla_\mu\nabla_\nu)f_R$  vanishes and no propagating Yukawa/breathing mode appears at linear order.
- **Background expansion.** The factor  $(1 - \lambda/8\pi)$  rescaling the matter term in the Friedmann equation alters  $dV_c/dz$  by  $\lesssim 1\%$ , well below the  $\sim 50\%$  uncertainty in the merger rate density  $\mathcal{R}(M_1, M_2, z)$ .
- **Astrophysical growth of IMBHs.** The Eddington time scales as  $G_{\text{eff}}^{-1}$ , so final masses change by  $\lesssim 1\%$ , subdominant relative to the scatter already assumed in the mass function. Additionally, deviations in the gravitational mass-luminosity relation can introduce corrections to the amplitude of gravitational waves due to the coupling between curvature and matter content.
- **High-pressure corrections.** The additional  $\lambda p g_{\mu\nu}$  term matters only inside compact stars or the merger remnant and has no impact on the inspiral phase observed by LISA or AMIGO.

Hence, for couplings consistent with all current local and astrophysical tests, the amplitude rescaling captured by  $\alpha(\lambda)$  suffices for robust detection-rate forecasts. Larger deviations would either break those bounds or require a screening mechanism, and are left for future work.

## 5 Discussion and Conclusions

### 5.1 Key findings

Combining an empirically motivated IMBH population model with updated sensitivity curves for LISA and the deci-Hz mission concept AMIGO, we have produced the first side-by-side forecast of detection bands, event counts and redshift distributions for *intermediate-mass* black-hole mergers under both General Relativity and its minimal matter-coupled extension  $f(R, T) = R + 2\lambda T$ . The main quantitative results are:

1. A redshift-dependent binary mass function  $\Phi(M_1, M_2, z)$ —anchored to the observed SMBH relation and folded with a Peters-based time-to-coalescence—predicts  $\sim 6 \times 10^6$  IMBH binaries within the observable Universe (Section 3.6).
2. In GR, LISA is most sensitive to  $M_{\text{tot}} \sim 10^4 - 10^6 M_\odot$  with a detection peak at  $z \simeq 4 - 5$ , while AMIGO excels at  $10^2 - 10^4 M_\odot$  and  $z \simeq 1.5 - 2$  (see Fig. 1). Together they provide continuous coverage from  $\approx 0.2$  Hz to 50 mHz.
3. Adopting Solar-System-compatible values  $|\lambda| \leq 2 \times 10^{-3}$ , the  $f(R, T)$  model rescales the strain by  $\alpha(\lambda) = (1 - \lambda/8\pi)^{5/6}$ . This shifts the LISA and AMIGO detection probabilities by  $\lesssim 1\%$  in redshift and changes the total event counts by  $\lesssim 5\%$  (Fig. 3).

4. Even with that small correction, *absolute* numbers remain high:  $\sim 10^4$  IMBH mergers for LISA over a four-year mission and hundreds-to-thousands for AMIGO in three years (fiducial scenario).
5. Other  $f(R, T)$  effects—phase shifts, Yukawa tails, density-dependent  $G$ , background expansion—enter at sub-percent level for the same  $\lambda$  and are therefore negligible for population-level statistics, though important for precision waveform tests (§4.4).

## 5.2 Astrophysical implications

High event rates at  $z > 4$  make IMBH mergers promising probes of early black-hole seeding and growth, complementing high-redshift quasars and direct-collapse scenarios [3]. The overlap of LISA and AMIGO in the  $10^3$ – $10^4 M_\odot$  range also opens a multiband detection channel when combined with the forthcoming *Einstein Telescope* (ET) and *Cosmic Explorer* (CE) ground observatories, allowing sky localisation to within a few square degrees and greatly facilitating electromagnetic follow-ups.

## 5.3 Modified gravity as a consistency check

Within the tight Solar-System bounds on  $\lambda$ , the linear  $f(R, T)$  model is indistinguishable from GR at the level of event counts. Nonetheless, the global amplitude rescaling offers a *consistency test*: after marginalising over astrophysical uncertainties, a systematic offset of a few percent between observed and predicted merger rates could hint at matter-geometry couplings or at other extensions that mimic a varying Newton constant.

## 5.4 Future work

- **Beyond linear  $f(R, T)$ .** Non-linear choices (e.g.  $R^2$ ,  $RT$ ,  $T^2$ ) can yield order-10% effects if equipped with screening to satisfy local tests [54, 55]. We plan to extend the present framework to those cases, including frequency- and density-dependent corrections to the waveform phase.
- **Self-consistent cosmology.** A full numerical treatment of the modified Friedmann equation would allow us to quantify how the small  $(1 - \lambda/8\pi)$  rescaling propagates into comoving volume, duty cycle and stochastic backgrounds.
- **Population inference.** Bayesian hierarchical modelling that fits the IMBH mass function *and* the coupling  $\lambda$  simultaneously could turn future LISA/AMIGO catalogues into competitive tests of gravity.

## 5.5 Conclusions

Our analysis confirms that space-based detectors will open a decisive window on the IMBH regime, providing thousands of sources across cosmic time. In the simplest matter-coupled gravity scenario, deviations from GR at the level permitted by Solar-System tests leave those prospects essentially intact, acting more as a self-consistency gauge than as a game-changing effect. Should nature choose a more intricate form of  $f(R, T)$  with efficient screening, detectable signatures—both in event statistics and in waveform phasing—remain a tantalizing possibility for future work.

## Acknowledgments

M.M.L. thanks Prof. Pedro H.R.S. Moraes for the constant encouragement that led to the initial steps of this work.

## References

- [1] B.P.A. et al., *Observation of gravitational waves from a binary black hole merger*, *Phys. Rev. Lett.* **116** (2016) 061102.
- [2] M.C. Miller and E.J.M. Colbert, *Intermediate-mass black holes*, *Int. J. Mod. Phys. D* **13** (2004) 1.
- [3] J.E. Greene, J. Strader and L.C. Ho, *Intermediate-mass black holes*, *Ann. Rev. Astron. Astrophys.* **58** (2020) 257.
- [4] J.C.N. de Araujo, O.D. Miranda and O.D. Aguiar, *Possible strong gravitational wave sources for the lisa antenna*, *Astrophys. J.* **550** (2001) 368.
- [5] E.S. Pereira and O.D. Miranda, *Supermassive black holes: connecting the growth to the cosmic star formation rate*, *Mon. Not. Roy. Astron. Soc. Lett.* **418** (2011) L30.
- [6] E.S. Pereira and O.D. Miranda, *Accretion history of active black holes from type 1 agn*, *Astrophys. Space Sci.* **352** (2014) 801.
- [7] E.S. Pereira and O.D. Miranda, *Stochastic background of gravitational waves generated by pregalactic black holes*, *Mon. Not. Roy. Astron. Soc.* **401** (2010) 1924.
- [8] O.D. Miranda, *Stochastic backgrounds of gravitational waves from cosmological sources – the role of dark energy*, *Mon. Not. Roy. Astron. Soc.* **426** (2012) 2758.
- [9] S.F.P. Zwart and S.L.W. McMillan, *The runaway growth of intermediate-mass black holes in dense star clusters*, *Astrophys. J.* **576** (2002) 899.
- [10] P. Madau and M.J. Rees, *Massive black holes as population iii remnants*, *Astrophys. J. Lett.* **551** (2001) L27.
- [11] M. Volonteri, *Formation of supermassive black holes*, *Astron. Astrophys. Rev.* **18** (2010) 279.
- [12] W.T. Ni, *Gravitational wave detection in space*, *Int. J. Mod. Phys. D* **25** (2016) 1630001.
- [13] P.A.-S. et al., *Laser interferometer space antenna*, *arXiv e-prints* (2017) [1702.00786].
- [14] A. Sesana, *Prospects for detection of gravitational waves from intermediate-mass black hole binaries in the nearby universe*, *Mon. Not. Roy. Astron. Soc.* **382** (2007) L6.
- [15] G. Fragione, I. Ginsburg and B. Kocsis, *Intermediate-mass ratio inspirals in galactic nuclei*, *Astrophys. J.* **856** (2018) 92.
- [16] K.W.K. Wong, T. Broadhurst and G.F. Smoot, *Testing the nature of black holes using lisa: prospects for probing the interior metric via gravitational lensing of gravitational waves*, *JCAP* **2021** (2021) 032.
- [17] F. Shankar, D.H. Weinberg and J. Miralda-Escudé, *Self-consistent models of the agn and black hole populations: duty cycles, accretion rates, and the mean radiative efficiency*, *Astrophys. J.* **690** (2009) 20.
- [18] P.B. et al., *Universe-machine: The correlation between galaxy growth and dark matter halo assembly from  $z = 0$  to 10*, *Mon. Not. Roy. Astron. Soc.* **488** (2019) 3143.
- [19] T. Harko, F.S.N. Lobo, S. Nojiri and S.D. Odintsov,  *$f(r, t)$  gravity*, *Phys. Rev. D* **84** (2011) 024020.

- [20] P.H.R.S. Moraes and P.K. Sahoo, *The simplest non-minimal matter–geometry coupling in  $f(r,t)$  gravity and some cosmological implications*, *Eur. Phys. J. C* **77** (2017) 480.
- [21] H. Shabani and M. Farhoudi,  *$f(r,t)$  cosmological models in the phase space*, *Phys. Rev. D* **90** (2014) 044031.
- [22] P.H.R.S. Moraes, J.D.V. Arbañil and M. Malheiro, *Stellar equilibrium in  $f(r,t)$  gravity*, *JCAP* **2016** (2016) 005.
- [23] D.D. et al, *Relativistic model for anisotropic strange stars in  $f(r,t)$  gravity*, *Ann. Phys.* **387** (2018) 239.
- [24] J.T. Quartuccio, P.H.R.S. Moraes, G.N. Zeminiani and M.M. Lapola, *The equilibrium configurations of neutron stars in the optimized  $f(r,t)$  gravity*, *Astrophys. Space Sci.* **370** (2025) 71.
- [25] P. Sahoo, P.H.R.S. Moraes, M.M. Lapola and P.K. Sahoo, *Traversable wormholes in the traceless  $f(r,t)$  gravity*, *Int. J. Mod. Phys. D* **30** (2021) 2150100.
- [26] M.E.S. Alves, P.H.R.S. Moraes, J.C.N. de Araujo and M. Malheiro, *Gravitational waves in  $f(r,t)$  and  $f(r,t\phi)$  theories of gravity*, *Phys. Rev. D* **94** (2016) 024032.
- [27] B.P.A. et al., *Gwtc-1: A gravitational-wave transient catalog of compact binary mergers observed by ligo and virgo during the first and second observing runs*, *Phys. Rev. X* **9** (2019) 031040.
- [28] R.A. et al., *Gwtc-2: Compact binary coalescences observed by ligo and virgo during the first half of the third observing run*, *Phys. Rev. X* **11** (2021) 021053.
- [29] A. Sesana, *Prospects for multiband gravitational-wave astronomy after gw150914*, *Phys. Rev. Lett.* **116** (2016) 231102.
- [30] M. Mapelli, *Massive black hole binaries from runaway collisions: the impact of metallicity*, *Mon. Not. Roy. Astron. Soc.* **459** (2016) 3432.
- [31] F. Antonini and F.A. Rasio, *Merging black hole binaries in galactic nuclei: implications for advanced ligo detections*, *Astrophys. J.* **831** (2016) 187.
- [32] K.B. et al., *Compact object modeling with the startrack population synthesis code*, *Astrophys. J. Suppl.* **174** (2008) 223.
- [33] A.S. et al., *The total merger rate of compact object binaries in the local universe*, *Astrophys. J.* **676** (2008) 1162.
- [34] I. Mandel and F.S. Broekgaarden, *Rates of compact object coalescences: comparisons between binary population synthesis and cosmological simulations*, *Mon. Not. Roy. Astron. Soc.* **481** (2018) 4009.
- [35] M.Z. et al., *Channeling the formation of compact object binaries: The impact of initial conditions on binary population synthesis*, *Astrophys. J.* **910** (2021) 152.
- [36] P.C. Peters, *Gravitational radiation and the motion of two point masses*, *Phys. Rev.* **136** (1964) B1224.
- [37] C.L.R. et al., *Dynamical formation of the gw150914 binary black hole*, *Astrophys. J. Lett.* **824** (2016) L8.
- [38] P.A. et al., *A template bank for gravitational waveforms from coalescing binary black holes. i. non-spinning binaries*, *Phys. Rev. D* **77** (2008) 104017 [0710.2335].
- [39] C.J. Moore, R.H. Cole and C.P.L. Berry, *Gravitational-wave sensitivity curves*, *Class. Quant. Grav.* **32** (2015) 015014 [1408.0740].
- [40] T. Robson, N.J. Cornish and C. Liu, *The construction and use of lisa sensitivity curves*, *Class. Quant. Grav.* **36** (2019) 105011 [1803.01944].

- [41] I. Mandel and S.E. de Mink, *Merging binary black holes formed through chemically homogeneous evolution in short-period stellar binaries*, *Mon. Not. Roy. Astron. Soc.* **458** (2016) 2634.
- [42] D. Gerosa and M. Fishbach, *Hierarchical mergers of stellar-mass black holes and their gravitational-wave signatures*, *Nature Astron.* **5** (2021) 749.
- [43] F.G. Alvarenga, A. de la Cruz-Dombriz, M.J.S. Houndjo, M.E. Rodrigues and D. Sáez-Gómez, *Dynamics of scalar perturbations in  $f(r, t)$  gravity*, *Phys. Rev. D* **87** (2013) 103526.
- [44] S.D. Odintsov and D. Sáez-Gómez,  *$f(r, t)$  gravity: an updated review*, *Universe* **7** (2021) 200.
- [45] D. Singh, S. Mandal, F. Rahaman, B.K. Guha and S. Ray, *Neutron-star configurations in  $f(r, t)$  gravity*, *JCAP* **2020** (2020) 007.
- [46] R. Nagpal, A. Gupta, S.K.J. Pacif, S. Sharma and R. Myrzakulov, *Anisotropic strange stars in  $f(r, t)$  gravity*, *Phys. Rev. D* **102** (2020) 124059.
- [47] S.K. Sharma, A.K. Mishra and F. Rahaman, *Wave generation and propagation in  $f(r, t)$  gravity*, *Eur. Phys. J. C* **82** (2022) 23.
- [48] W.T. Ni, *Gravitational-wave classification, space gw detection sensitivities and the AMIGO mission concept*, *EPJ Web Conf.* **168** (2018) 01004 [1709.05659].
- [49] U. Debnath, *Gravitational lensing and shadows of a charged rotating black hole in  $f(r, t)$  gravity*, *Eur. Phys. J. C* **81** (2021) 632.
- [50] C.M. Will, *The confrontation between general relativity and experiment*, *Living Rev. Rel.* **17** (2014) 4.
- [51] B. Bertotti, L. Iess and P. Tortora, *A test of general relativity using radio links with the cassini spacecraft*, *Nature* **425** (2003) 374.
- [52] M.K. et al., *Tests of general relativity from timing the double pulsar*, *Science* **314** (2006) 97.
- [53] J.M. Weisberg and Y. Huang, *Relativistic measurements from timing the binary pulsar psr b1913+16*, *Astrophys. J.* **829** (2016) 55.
- [54] J. Khoury and A. Weltman, *Chameleon cosmology*, *Phys. Rev. D* **69** (2004) 044026.
- [55] E.H. Baffou, M.J.S. Houndjo and I.G. Salako, *Polarizations of gravitational waves in  $f(r, t)$  gravity*, *Astrophys. Space Sci.* **364** (2019) 90.